ADVANCED MATERIALS
www.advmat.de

A Nanosized CoNi Hydroxide@Hydroxysulfide Core–Shell Heterostructure for Enhanced Oxygen Evolution

*Bin Wang, Cheng Tang, Hao-Fan Wang, Xiao Chen, Rui Cao, and Qiang Zhang**

A cost-effective and highly efficient oxygen evolution reaction (OER) electrocatalyst will be significant for the future energy scenario. The emergence of the core–shell heterostructure has invoked new feasibilities to inspire the full potential of non-precious-metal candidates. The shells always have a large thickness, affording robust mechanical properties under harsh reaction conditions, which limits the full exposure of active sites with highly intrinsic reactivity and extrinsic physicochemical characters for optimal performance. Herein, a nanosized CoNi hydroxide@hydroxysulfide core–shell heterostructure is fabricated via an ethanol-modified surface sulfurization method. Such a synthetic strategy is demonstrated to be effective in controllably fabricating a core–shell heterostructure with an ultrathin shell (4 nm) and favorable exposure of active sites, resulting in a moderately regulated electronic structure, remarkably facilitated charge transfer, fully exposed active sites, and a strongly coupled heterointerface for energy electrocatalysis. Consequently, the as-obtained hydroxide@hydroxysulfide core–shell is revealed as a superior OER catalyst, with a small overpotential of 274.0 mV required for 10.0 mA cm^{-2}, a low Tafel slope of 45.0 mV dec^{-1}, and a favorable long-term stability in 0.10 M KOH. This work affords fresh concepts and strategies for the design and fabrication of advanced core–shell heterostructures, and thus opens up new avenues for the targeted development of high-performance energy materials.

The oxygen evolution reaction (OER) is one of the most important electrocatalytic processes for the future energy scenario, which is coupled with various renewable energy systems such as water splitting units,[1] metal–air batteries,[2] and solar cells.[3] Nevertheless, this reaction considerably suffers from its sluggish kinetics due to the multi-electron process nature ($4OH^- \rightarrow O_2 + 2H_2O + 4e^-$, in alkaline),[4] and thereby exhibits high overpotential and low energy efficiency. To date, precious metal oxides, such as IrO_2 and RuO_2, still hold the benchmarking activity for electrocatalytic OER,[5,6] but the practical application is greatly inhibited by their high cost, low abundance, and insufficient stability. Therefore, it is highly desirable to develop greatly effective and robust OER catalysts based on earth-abundant elements.[7] Emerging as a versatile family of outstanding alternatives, transition metal compounds have recently drawn particular attention due to their high-performance, cost-efficient, structure-tunable, and environment-benign features. Generally, their OER electrocatalytic activity can be efficiently optimized by electronic engineering, including cation regulation (Co^{3+},[8] Ni^{2+},[9,10] Fe^{3+},[11] Mn^{4+},[12] Mo^{6+},[13] etc.) and anion regulation (S^{2-},[14] P^{3-},[15] N^{3-},[16] S^{2-}/OH^-,[17–19] etc.), to alter the adsorption behavior and intrinsic activity. Besides, interface engineering with favorable nanostructures (nanosized hybrid,[9,20] core–shell,[6,21,22] freestanding,[23] etc.) is also of great benefit to the electrocatalysis performance by improving the conductivity, facilitating the charge transfer, and generating strong couple effects.

Specifically, the recent attention on core–shell heterostructures invokes emerging feasibilities to thoroughly demonstrate the full potential of transition metal compounds in OER electrocatalysis. By coupling two components with different compositions and crystallinities, the constructed core–shell heterostructure is expected to achieve synergistic effects with electronic and interface engineering simultaneously, such as CoO_x/CoP,[24] MoS_2/Ni_3S_2,[25] Ni_2P/NiO_x,[26] $NiPS_3$@NiOOH,[27] $CoFe_2O_4$@CoFeBi,[28] and so on. The heterogeneous shell and interface are able to modulate the electronic structure,[27] endow highly active surface,[25] decrease interfacial contact resistance,[29] and boost charge transfer,[30] thereby leading to greatly enhanced electrocatalytic performance. It is obvious that the features of the shell, including composition, thickness, porosity, and crystallinity, will play a vital role in regulating the resultant reactivity. Nevertheless, these core–shell heterostructures are mainly fabricated under harsh conditions or uncontrollably formed in situ during electrocatalysis,[31] which lack capability to precisely control their characters. Therefore, smart design and versatile techniques are urgently required for the controllable construction of advanced core–shell heterostructures,

Dr. B. Wang, Dr. C. Tang, Dr. H.-F. Wang, Dr. X. Chen, Prof. Q. Zhang
Beijing Key Laboratory of Green Chemical Reaction Engineering and Technology
Department of Chemical Engineering
Tsinghua University
Beijing 100084, China
E-mail: zhang-qiang@mails.tsinghua.edu.cn
Prof. R. Cao
School of Chemistry and Chemical Engineering
Shaanxi Normal University
Xi'an 710119, China
The ORCID identification number(s) for the author(s) of this article can be found under https://doi.org/10.1002/adma.201805658.

DOI: 10.1002/adma.201805658

aiming at high intrinsic catalytic activity and suitable extrinsic physicochemical characters for optimal OER performance.

Here, we report the design a hydroxide@hydroxysulfide core–shell heterostructure and devise an ethanol-modified surface sulfurization method to facilely synthesize such heterostructure material. Well-developed CoNi hydroxide sheets were synthesized in advance, and then an ultrathin CoNi hydroxysulfide shell was controllably generated on the hydroxide surface with the formation of a core–shell heterostructure. The as-proposed strategy is demonstrated effectively to precisely control the nanostructure and effectively regulate the electronic structure. As a result, the CoNi based hydroxide@hydroxysulfide core–shell heterostructure was revealed to exhibit a superior OER performance, with high activities, rapid kinetics, and excellent durability in alkaline condition. The material design and synthetic strategy herein are believed to afford emerging opportunities and inspiration in the field of core–shell heterostructures for various energy applications.

The CoNi hydroxide@hydroxysulfide (denoted as $Co_{1.8}Ni(OH)_{5.6}@Co_{1.8}NiS_{0.4}(OH)_{4.8}$) core–shell heterostructure was fabricated via an ethanol-modified surface sulfurization as schematically illustrated in **Figure 1**. First, high-quality and regular-shaped CoNi hydroxide (denoted as $Co_{1.8}Ni(OH)_{5.6}$) nanosheets were prepared through a homogeneous precipitation of dilute $CoCl_2$ and $NiCl_2$ solutions with hexamethylenetetramine (HMT) under Ar protection. The exclusion of O_2 and CO_2 by Ar flow and the slow nucleation ascribed to the prolonged HMT hydrolysis are crucial to guarantee the uniform hexagonal morphology, large size, and high crystallinity of as-obtained $Co_{1.8}Ni(OH)_{5.6}$ (Figure S1, Supporting Information), which facilitates a rational and precise control of the subsequent surface sulfurization. Then the as-obtained $Co_{1.8}Ni(OH)_{5.6}$ sample was immersed in 2.0 M Na_2S ethanol solution for 24.0 h under room temperature. During this process, the $Co_{1.8}Ni(OH)_{5.6}$ platelets undergo an interfacial reaction with hydrolyzed HS^- and thus transformation into a CoNi hydroxysulfide shell ($S^{2-} + C_2H_5OH \rightarrow HS^- + C_2H_5O^-$, $Co_{1.8}Ni(OH)_{5.6} + HS^- \rightarrow$ CoNi hydroxysulfide), due to significantly different solubilities (K_{sp}) between the sulfide and hydroxide (see details in the Supporting Information).[17] Notably, ethanol was employed as the solvent rather than routine water during the sulfurization process to decrease the rate of Na_2S dissociation and interfacial reaction, thereby ensuring the precise modulation on the resultant nanosized $Co_{1.8}Ni(OH)_{5.6}@Co_{1.8}NiS_{0.4}(OH)_{4.8}$ core–shell heterostructure. A counterpart hydroxysulfide (denoted as $Co_{1.7}NiS_{1.6}(OH)_{2.2}$) deeply sulfurized in 2.0 M Na_2S aqueous solution was also fabricated under otherwise identical conditions.

To reveal the nanosized morphology and core–shell heterostructure, transmission electron microscopy (TEM) characterization was carried out. As shown in **Figure 2**a and Figure S2 in the Supporting Information, the as-obtained $Co_{1.8}Ni(OH)_{5.6}@Co_{1.8}NiS_{0.4}(OH)_{4.8}$ sample presents a well-maintained hexagonal plate-like morphology of the $Co_{1.8}Ni(OH)_{5.6}$ precursors with a lateral size of ≈1.5 µm, which is attributed to the mild sulfurization conditions. Figure S3 in the Supporting Information presents the results of atomic force microscopy, which further indicates a uniform thickness of 39.5 (± 2.7) nm for $Co_{1.8}Ni(OH)_{5.6}@Co_{1.8}NiS_{0.4}(OH)_{4.8}$, consistent with the scanning electron microscopy (SEM) results (Figure S4, Supporting Information). The selected area electron diffraction (SAED) pattern obtained from an individual $Co_{1.8}Ni(OH)_{5.6}@Co_{1.8}NiS_{0.4}(OH)_{4.8}$ sheet (Figure 2b, inset) displays a clear set of hexagonally arranged spots assigned to $Co_{1.8}Ni(OH)_{5.6}$ hydroxides (Figure S1c, Supporting Information), indicating a hydroxide bulk nature maintained in the $Co_{1.8}Ni(OH)_{5.6}@Co_{1.8}NiS_{0.4}(OH)_{4.8}$ heterostructure. Meanwhile, in contrast to the smooth surface of $Co_{1.8}Ni(OH)_{5.6}$ (Figure S1b, Supporting Information), a cotton-like surface was observed in $Co_{1.8}Ni(OH)_{5.6}@Co_{1.8}NiS_{0.4}(OH)_{4.8}$ by high-angle annular dark-field scanning transmission electron microscopy (HAADF-STEM) images (Figure 2b and Figure S5, Supporting Information), suggesting the formation of a crystalline disordered hydroxysulfide shell. The incorporation of sulfur into the hydroxide matrix is believed to induce moderate lattice mismatch and distortion,[32] thereby leading to the lack of long-range crystalline order and generation of the crystalline disordered structure in both $Co_{1.8}Ni(OH)_{5.6}@Co_{1.8}NiS_{0.4}(OH)_{4.8}$ and $Co_{1.7}NiS_{1.6}(OH)_{2.2}$ samples (Figures S5–S7). The N_2 adsorption/desorption analysis indicates a prominently higher specific surface area (122.7 $m^2\ g^{-1}$) and larger pore volume (0.155 $cm^3\ g^{-1}$) of $Co_{1.8}Ni(OH)_{5.6}@Co_{1.8}NiS_{0.4}(OH)_{4.8}$ than those of $Co_{1.8}Ni(OH)_{5.6}$ precursors (87.3 $m^2\ g^{-1}$ and 0.082 $cm^3\ g^{-1}$, respectively). This is mainly contributed by the remarkably increased mesopores around 4 nm, which is ascribed to the generated cotton-like surface (Figure S8, Supporting Information).

The hydroxide@hydroxysulfide core–shell heterostructure was further confirmed by the elaborate characterization of element distributions. As displayed in Figure S9 in the Supporting Information, the energy dispersive spectrum (EDS) mapping of a deeply sulfurized $Co_{1.7}NiS_{1.6}(OH)_{2.2}$ nanosheet exhibits a uniform distribution of S element overlapping Co,

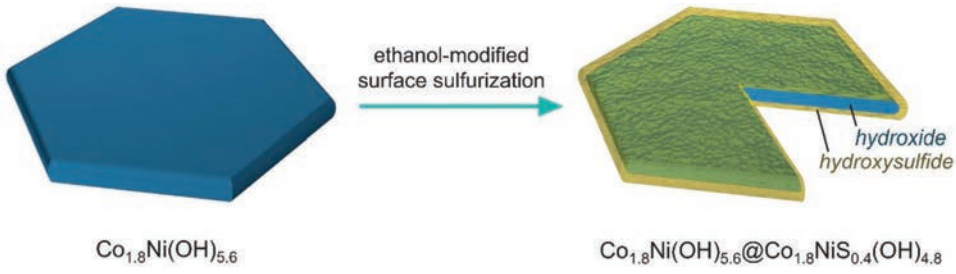

Figure 1. Schematic illustration of the ethanol-modified surface sulfurization process for the fabrication of $Co_{1.8}Ni(OH)_{5.6}@Co_{1.8}NiS_{0.4}(OH)_{4.8}$ core–shell heterostructures.

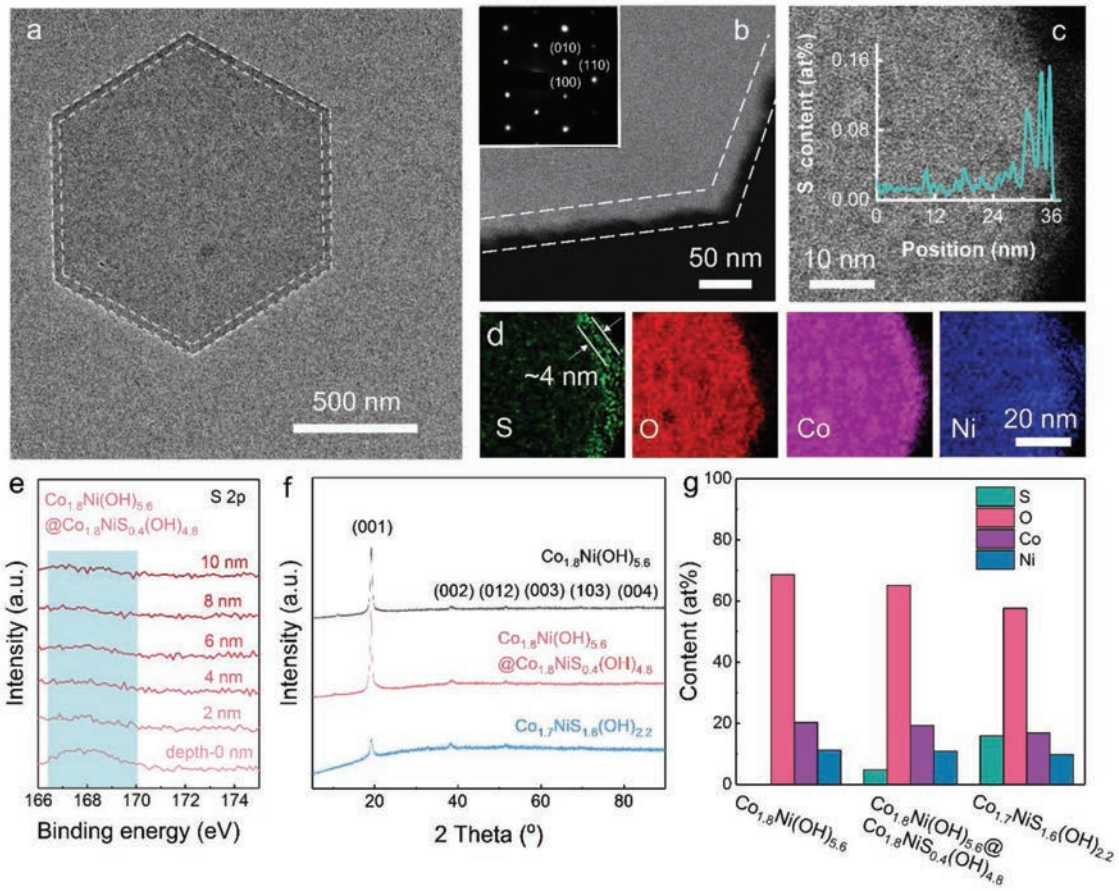

Figure 2. Characterizations of $Co_{1.8}Ni(OH)_{5.6}$@$Co_{1.8}NiS_{0.4}(OH)_{4.8}$ core–shell heterostructure. a) TEM image. b) HAADF-STEM image and SAED pattern (inset). c) HAADF-STEM image and corresponding EDS line scan. d) EDS mapping. e) High-resolution depth-profiling XPS spectra of S 2p. f) XRD patterns of all samples. g) Elemental composition detected by XPS analysis.

Ni, and O elements on the whole sheet. In contrast, a distinct sulfur-rich shell is clearly observed on the $Co_{1.8}Ni(OH)_{5.6}$@$Co_{1.8}NiS_{0.4}(OH)_{4.8}$ sheet in both the line-scan (Figure 2c) and elemental mapping results (Figure 2d). Such difference incontrovertibly manifests the core–shell textural nature for this $Co_{1.8}Ni(OH)_{5.6}$@$Co_{1.8}NiS_{0.4}(OH)_{4.8}$ heterostructure, which is further verified by the depth-profiling X-ray photoelectron spectroscopy (XPS) analysis. As shown in Figure 2e, the S 2p peak around 168.0 eV is evident in the $Co_{1.8}Ni(OH)_{5.6}$@$Co_{1.8}NiS_{0.4}(OH)_{4.8}$ surface, but gradually decreases with a deeper probing depth, and finally disappears in bulk analysis. Inspiringly, attributed to the precisely controllable ethanol-modified sulfurization strategy, the thickness of this continuous and cotton-like hydroxysulfide shell is less than 4 nm according to the EDS and XPS analysis, smaller than most core–shell materials reported previously.[26,33]

To further investigate the sulfurization process and composition transformation, the crystal phase and composition of all samples were probed by X-ray diffraction (XRD) and XPS measurements. The XRD pattern of $Co_{1.8}Ni(OH)_{5.6}$ reveals a brucite structure with hexagonal lattice parameters of a = 0.3153 nm and c = 0.4632 nm (Figure 2f).[34] After surface sulfurization in Na_2S ethanol solution, no obvious difference can be observed for $Co_{1.8}Ni(OH)_{5.6}$@$Co_{1.8}NiS_{0.4}(OH)_{4.8}$, suggesting a slight transformation degree. In contrast, after deep sulfurization in Na_2S aqueous solution, the peak intensity is evidently decreased for $Co_{1.7}NiS_{1.6}(OH)_{2.2}$, indicating a large-scale transformation of crystalline hydroxides into amorphous hydroxysulfides. This result also highlights the critical role of the ethanol-modified sulfurization on the precise control of the $Co_{1.8}Ni(OH)_{5.6}$@$Co_{1.8}NiS_{0.4}(OH)_{4.8}$ core–shell heterostructure. Figure 2g summarizes the element contents of all samples determined from the XPS surveys (Figure S10 and Table S2, Supporting Information). It is revealed that with the increase of the sulfurization degree, the S content increases as expected (4.8 at% for $Co_{1.8}Ni(OH)_{5.6}$@$Co_{1.8}NiS_{0.4}(OH)_{4.8}$ and 15.9 at% for $Co_{1.7}NiS_{1.6}(OH)_{2.2}$), and the O content decreases (68.6 at% for $Co_{1.8}Ni(OH)_{5.6}$, 65.1 at% for $Co_{1.8}Ni(OH)_{5.6}$@$Co_{1.8}NiS_{0.4}(OH)_{4.8}$, and 57.6 at% for $Co_{1.7}NiS_{1.6}(OH)_{2.2}$), indicating the gradual replacement of O by S element and transformation of hydroxides to hydroxysulfides.

The characterizations above strongly indicate the successful synthesis of precisely-controlled $Co_{1.8}Ni(OH)_{5.6}$@$Co_{1.8}NiS_{0.4}(OH)_{4.8}$ core–shell heterostructure by the ethanol-modified surface sulfurization. With a well preservation of the bulk hydroxide core, an ultrathin cotton-like hydroxysulfide shell less than 4 nm is generated via a moderate interfacial reaction. Along with the regulated electronic structure, cotton-like surface shell, fully exposed active sites, and strongly

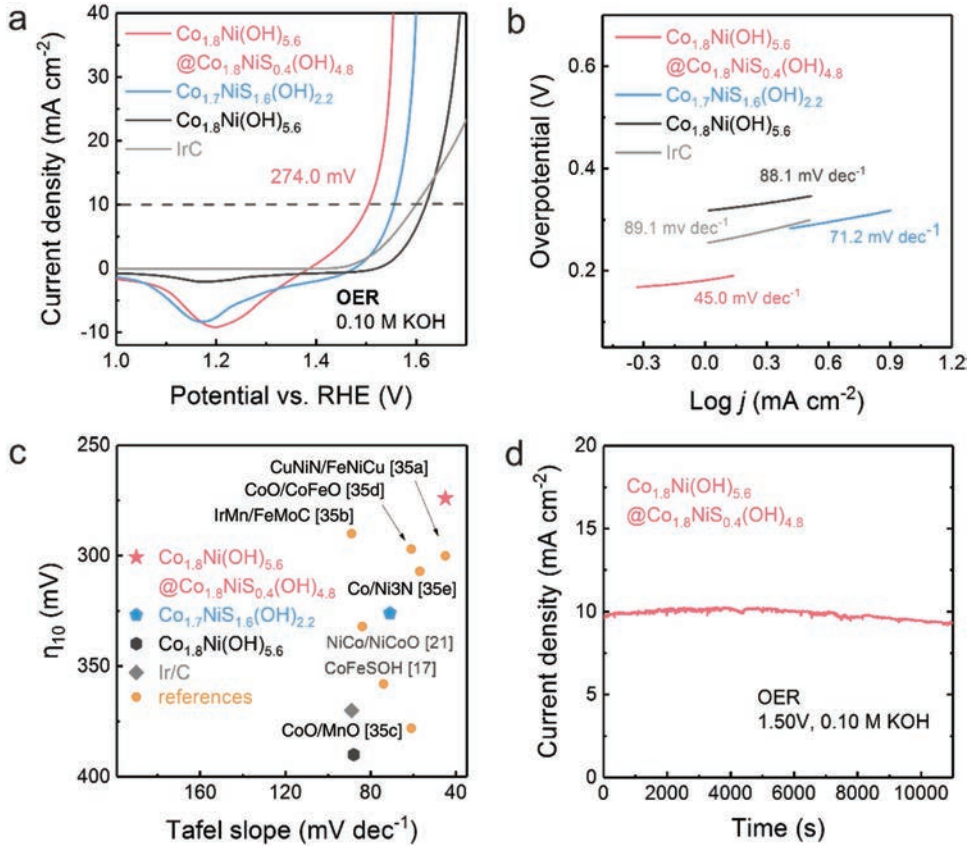

Figure 3. OER performances of $Co_{1.8}Ni(OH)_{5.6}@Co_{1.8}NiS_{0.4}(OH)_{4.8}$ and control samples in O_2-satuated 0.10 M KOH electrolyte. a) LSV curves obtained with a scan rate of 5.0 mV s^{-1}. The horizontal axis represents the potential versus reversible hydrogen electrode (RHE). b) Tafel plots. c) Figure of merit with respect to both activity (the overpotential required to achieve 10 mA cm^{-2}) and kinetics (Tafel slope), with references all measured in alkaline electrolyte. d) Chronoamperometric response at an overpotential of 270 mV.

coupled heterointerfaces, $Co_{1.8}Ni(OH)_{5.6}@Co_{1.8}NiS_{0.4}(OH)_{4.8}$ is expected to be an attractive alternative for OER electrocatalysis.

The electrocatalytic performance of the as-obtained $Co_{1.8}Ni(OH)_{5.6}@Co_{1.8}NiS_{0.4}(OH)_{4.8}$ core–shell heterostructure was investigated in 0.10 M KOH on a three-electrode configuration with an areal loading of 0.25 mg cm^{-2}. To avoid the influence of the oxidation current of Co^{2+} and Ni^{2+} to Co^{3+} and Ni^{3+}, respectively, the linear sweep voltammetry (LSV) polarization curves were swept from the high to low potential.[32] As shown in **Figure 3**a, $Co_{1.8}Ni(OH)_{5.6}@Co_{1.8}NiS_{0.4}(OH)_{4.8}$ exhibits the lowest overpotential of 274.0 mV at 10 mA cm^{-2} (η_{10}). It is much lower than $Co_{1.8}Ni(OH)_{5.6}$ (390.2 mV), $Co_{1.7}NiS_{1.6}(OH)_{2.2}$ (326.1 mV), and the commercial Ir/C catalyst (370.1 mV), indicating a superior OER activity of the $Co_{1.8}Ni(OH)_{5.6}@Co_{1.8}NiS_{0.4}(OH)_{4.8}$ heterostructure. Tafel slope was employed to investigate the OER kinetics.[9] As drawn in Figure 3b, $Co_{1.8}Ni(OH)_{5.6}@Co_{1.8}NiS_{0.4}(OH)_{4.8}$ exhibits a Tafel slop as low as 45.0 mV dec^{-1}, which is much smaller than other catalysts (71.2–89.1 mV dec^{-1}). The catalyst with a lower Tafel slope favors accelerating the OER process with improved kinetics. As a result, $Co_{1.8}Ni(OH)_{5.6}@Co_{1.8}NiS_{0.4}(OH)_{4.8}$ can deliver a higher current density driven by the same overpotential, and achieve a high current density of 40.0 mA cm^{-2} at an overpotential of 324.0 mV, which is over sevenfold that of Ir/C catalyst (Figure 3a). With regard to both activity and kinetics, $Co_{1.8}Ni(OH)_{5.6}@Co_{1.8}NiS_{0.4}(OH)_{4.8}$ is demonstrated as an outstanding OER electrocatalyst, which is remarkably superior to $Co_{1.8}Ni(OH)_{5.6}$ and $Co_{1.7}NiS_{1.6}(OH)_{2.2}$), and also among the best results of similar materials reported so far (Figure 3c and Table S1, Supporting Information).[11,17,21,35]

It is widely accepted that the catalyst surface undergoes considerable transformation under oxidizing potentials during OER,[26,27] which is more noteworthy in the case of transition metal sulfides/hydroxysulfides.[31] Therefore, the long-term durability of $Co_{1.8}Ni(OH)_{5.6}@Co_{1.8}NiS_{0.4}(OH)_{4.8}$ was further investigated at a constant overpotential of 270 mV, and the structure and composition of the sample after electrocatalysis were characterized by TEM and XPS. As shown in Figure S11 in the Supporting Information, the hexagonal plate-like morphology of $Co_{1.8}Ni(OH)_{5.6}@Co_{1.8}NiS_{0.4}(OH)_{4.8}$ is well preserved after long-term OER. A part of Co^{2+} and Ni^{2+} in the original $Co_{1.8}Ni(OH)_{5.6}@Co_{1.8}NiS_{0.4}(OH)_{4.8}$ sample is converted into Co^{3+} and Ni^{3+} (Figure S12, Supporting Information), which is widely observed on hydroxide-based OER electrocatalysts.[36] Notably, the S content is slightly reduced during the OER process due to the sulfur redox (Figure S13, Supporting Information),[37] which is measured to be ≈2.0 at% by both EDS and XPS and about 42% of the original one (4.8 at%). It indicates that the CoNi hydroxysulfide shell may experience a mild reorganization during OER toward a more stable and active phase.

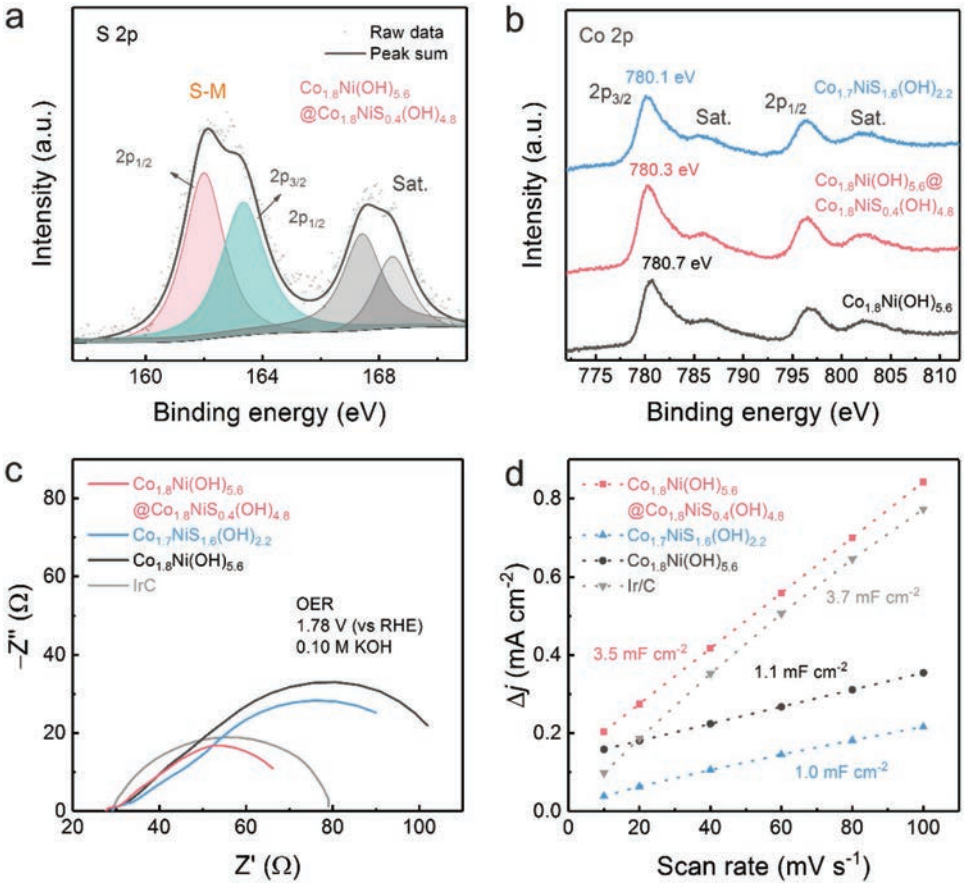

Figure 4. Enhanced OER performances arising from the novel structural features. a) High-resolution S 2p XPS spectrum of $Co_{1.8}Ni(OH)_{5.6}$@$Co_{1.8}NiS_{0.4}(OH)_{4.8}$. b) High-resolution Co 2p XPS spectra of $Co_{1.8}Ni(OH)_{5.6}$@$Co_{1.8}NiS_{0.4}(OH)_{4.8}$ and control samples. c) Nyquist plots obtained from EIS measurements at a potential of 1.78 V versus RHE. d) Charging current density differences plotted against scan rates. The linear slope, equivalent to twice the double-layer capacitance C_{dl}, is employed to represent the ECSA.

Consequently, $Co_{1.8}Ni(OH)_{5.6}$@$Co_{1.8}NiS_{0.4}(OH)_{4.8}$ exhibits a good long-term durability for OER process around the current density of ≈10 mA cm^{-2} (Figure 3d). The slight increase of the response current density before 5000 s can be ascribed to the in situ gained surface area and active sites from the sulfur redox.[37,38]

The superior OER electrocatalytic activity of $Co_{1.8}Ni(OH)_{5.6}$@$Co_{1.8}NiS_{0.4}(OH)_{4.8}$ can be first attributed to the electronic engineering effect derived by anion regulation (S^{2-}/OH^{-}).[18,39] Because sulfur has higher polarization ability and lower electronegativity than oxygen, the moderate replacement of oxygen by sulfur is able to regulate the electronic structure toward optimal intrinsic OER activities.[17,40] The incorporated sulfur in $Co_{1.8}Ni(OH)_{5.6}$@$Co_{1.8}NiS_{0.4}(OH)_{4.8}$ is shown to interact with metal cations in the hydroxysulfide phase (**Figure 4**a). Compared with oxygen, sulfur can afford more electrons to the 3d orbits of Co and Ni, thus modifying the electronic structure of active sites. However, its excessive incorporation by deep sulfurization will result in a too negative electronic field, which is unfavorable for OER on the contrary. As shown in Figure 4b, the Co 2p peaks of three samples gradually shift to lower binding energies with the increase of S contents. The sulfur atoms afford more electrons than those of original one in pristine $Co_{1.8}Ni(OH)_{5.6}$ hydroxides. However, the $Co_{1.8}Ni(OH)_{5.6}$@$Co_{1.8}NiS_{0.4}(OH)_{4.8}$ sample with a relatively small shift exhibits the best OER activity. Besides, though the S content in $Co_{1.8}Ni(OH)_{5.6}$@$Co_{1.8}NiS_{0.4}(OH)_{4.8}$ (4.8 at%) is less than one-third of that in $Co_{1.7}NiS_{1.6}(OH)_{2.2}$ (15.9 at%), the former OER activity and kinetics are significantly superior to those of $Co_{1.7}NiS_{1.6}(OH)_{2.2}$. These results suggest the remarkable importance of the unique core–shell heterostructure in addition to the anion regulation on the activity enhancement.

To gain more insights into the roles of sulfur incorporation and core–shell heterostructure in promoting the OER activity, the electrochemical impedance spectroscopy (EIS) and electrochemically active surface (ECSA) of all samples were explored. As revealed in Figure 4c, the charge transfer resistance of $Co_{1.7}NiS_{1.6}(OH)_{2.2}$ is smaller than $Co_{1.8}Ni(OH)_{5.6}$, and that of $Co_{1.8}Ni(OH)_{5.6}$@$Co_{1.8}NiS_{0.4}(OH)_{4.8}$ is further decreased. On the one hand, the suitable incorporation of sulfur with higher polarizability and less electronegativity than original oxygen is able to improve the charge transfer through inducing the delocalization of metal d-electrons.[41] On the other hand, the ultrathin hydroxysulfide shell and strongly coupled heterointerfaces may also alter the electronic structure and benefit the charge transfer. Consequently, more CoNi species in $Co_{1.8}Ni(OH)_{5.6}$@$Co_{1.8}NiS_{0.4}(OH)_{4.8}$ can be converted into high-valence cations

during the OER process, suggested by the larger redox peak in LSV (Figures S12 and S14, Supporting Information). The high-valence metal species, like NiOOH and CoOOH, possess superior activity to low-valence ones,[42] thereby leading to an enhanced OER activity.

The ECSA is represented by the electrochemical double-layer capacitance (C_{dl}). As discussed earlier, the surface sulfurization leads to the formation of a cotton-like crystalline disordered hydroxysulfide shell, and the disordered extent can be further boosted by the sulfur redox conversion during OER electrocatalysis. Consequently, $Co_{1.8}Ni(OH)_{5.6}@Co_{1.8}NiS_{0.4}(OH)_{4.8}$ delivers an apparently higher ECSA than $Co_{1.8}Ni(OH)_{5.6}$ (Figure 4d). The much lower ECSA of $Co_{1.7}NiS_{1.6}(OH)_{2.2}$ can be rationalized by the aggregation of sulfurized clusters and stacking of the hydroxysulfide sheets induced by the excessive sulfurization treatment.[43] Therefore, the $Co_{1.8}Ni(OH)_{5.6}@Co_{1.8}NiS_{0.4}(OH)_{4.8}$ sample affords a favorable surface with abundant and fully accessible active sites. Meanwhile, the coupling of such defective hydroxysulfide shell with relatively stable hydroxide core also plays a vital role in enhancing the electrocatalytic durability compared with $Co_{1.8}Ni(OH)_{5.6}$ and $Co_{1.7}NiS_{1.6}(OH)_{2.2}$ (Figure S15, Supporting Information).

The CoNi core–shell heterostructure was constructed with an ultrathin cotton-like hydroxysulfide shell uniformly in situ generated on the plate-like hydroxide surface, with the formation of highly active heterointerfaces. First, the controllably incorporated sulfur suitably regulates the electronic structure, leading to a high intrinsic electrocatalytic activity. Second, the formation of the ultrathin cotton-like structure facilitates full exposure of active sites and highly active heterointerfaces. Additionally, the delocalization of the metal d-electrons induced by introduced sulfur and strongly coupled interface greatly facilitate charge transfer process. Furthermore, the stable core–shell heterostructure contributes to an obviously improved electrocatalytic durability. Taken together, the synergy of the high intrinsic activity and favorable extrinsic characters make it an attractive electrocatalyst for OER process.

In summary, a $Co_{1.8}Ni(OH)_{5.6}@Co_{1.8}NiS_{0.4}(OH)_{4.8}$ core–shell heterostructure has been proposed and fabricated by an ethanol-modified surface sulfurization, aiming at a fully enhanced OER performance for CoNi compounds. The cotton-like crystalline disordered hydroxysulfide shell can be controlled as thin as 4 nm due to the moderative interfacial reaction. The as-obtained $Co_{1.8}Ni(OH)_{5.6}@Co_{1.8}NiS_{0.4}(OH)_{4.8}$ was demonstrated as a superior OER catalyst, with a remarkably decreased overpotential (274.0 mV required for 10.0 mA cm^{-2}), a significantly low Tafel slope (45.0 mV dec^{-1}), and a favorable long-term stability. It is ascribed to the synergistic effects of the electronic engineering by the sulfur incorporation and interface engineering by the core–shell heterostructure, including moderately regulated electronic structure, remarkably facilitated charge transfer, fully exposed active sites, and strongly coupled heterointerface. The design principle and synthetic strategy for such core–shell heterostructure present in this work are inspiring and applicable for a wide range of materials, and expected to open up new avenues for the development of advanced materials for various energy applications, such as water splitting, batteries, nitrogen reduction, and so on.

Supporting Information

Supporting Information is available from the Wiley Online Library or from the author.

Acknowledgements

B.W. and C.T. contributed equally to this work. This work was supported by National Key Research and Development Program (2016YFA0202500 and 2016YFA0200101), Natural Scientific Foundation of China (21825501), and Tsinghua University Initiative Scientific Research Program. The authors thank Bo-Quan Li, Xiao-Yang Cui, Xiao-Meng Liu, and Ling Zhong for helpful discussion.

Conflict of Interest

The authors declare no conflict of interest.

Keywords

core–shell structures, electrocatalysis, heterostructures, hydroxysulfides, oxygen evolution reaction

Received: August 31, 2018
Revised: November 16, 2018
Published online: December 5, 2018

[1] a) J. Wang, W. Cui, Q. Liu, Z. Xing, A. M. Asiri, X. Sun, *Adv. Mater.* **2016**, *28*, 215; b) J. Feng, F. Lv, W. Zhang, P. Li, K. Wang, C. Yang, B. Wang, Y. Yang, J. Zhou, F. Lin, G.-C. Wang, S. Guo, *Adv. Mater.* **2017**, *29*, 1703798.
[2] a) J. Fu, Z. P. Cano, M. G. Park, A. Yu, M. Fowler, Z. Chen, *Adv. Mater.* **2017**, *29*, 1604685; b) J. Fu, F. M. Hassan, C. Zhong, J. Lu, H. Liu, A. Yu, Z. Chen, *Adv. Mater.* **2017**, *29*, 1702526.
[3] S. Han, D. Wu, S. Li, F. Zhang, X. Feng, *Adv. Mater.* **2014**, *26*, 849.
[4] a) C. Tang, H.-F. Wang, X. Chen, B.-Q. Li, T.-Z. Hou, B. Zhang, Q. Zhang, M.-M. Titirici, F. Wei, *Adv. Mater.* **2016**, *28*, 6845; b) Y. Zhang, X. L. Fan, J. H. Jian, D. S. Yu, Z. S. Zhang, L. M. Dai, *Energy Environ. Sci.* **2017**, *10*, 2312; c) I. C. Man, H.-Y. Su, F. Calle-Vallejo, H. A. Hansen, J. I. Martínez, N. G. Inoglu, J. Kitchin, T. F. Jaramillo, J. K. Nørskov, J. Rossmeisl, *ChemCatChem* **2011**, *3*, 1085.
[5] a) Y. Zhang, C. Wu, H. Jiang, Y. Lin, H. Liu, Q. He, S. Chen, T. Duan, L. Song, *Adv. Mater.* **2018**, *30*, 1707522; b) H. G. Sanchez Casalongue, M. L. Ng, S. Kaya, D. Friebel, H. Ogasawara, A. Nilsson, *Angew. Chem., Int. Ed.* **2014**, *53*, 7169.
[6] Z. Zhuang, W. Sheng, Y. Yan, *Adv. Mater.* **2014**, *26*, 3950.
[7] a) N.-T. Suen, S.-F. Hung, Q. Quan, N. Zhang, Y.-J. Xu, H. M. Chen, *Chem. Soc. Rev.* **2017**, *46*, 337; b) J. Suntivich, K. J. May, H. A. Gasteiger, J. B. Goodenough, Y. Shao-Horn, *Science* **2011**, *334*, 1383; c) D. Yan, Y. Li, J. Huo, R. Chen, L. Dai, S. Wang, *Adv. Mater.* **2017**, *29*, 1606459; d) C. Spöri, J. T. H. Kwan, A. Bonakdarpour, D. P. Wilkinson, P. Strasser, *Angew. Chem., Int. Ed.* **2017**, *56*, 5994.
[8] a) C. Tang, B. Wang, H.-F. Wang, Q. Zhang, *Adv. Mater.* **2017**, *29*, 1703185; b) B.-Q. Li, S.-Y. Zhang, B. Wang, Z.-J. Xia, C. Tang, Q. Zhang, *Energy Environ. Sci.* **2018**, *11*, 1723.
[9] C. Tang, H.-S. Wang, H.-F. Wang, Q. Zhang, G.-L. Tian, J.-Q. Nie, F. Wei, *Adv. Mater.* **2015**, *27*, 4516.
[10] Y. Li, P. Hasin, Y. Wu, *Adv. Mater.* **2010**, *22*, 1926.

[11] a) J. Nai, Y. Lu, L. Yu, X. Wang, X. W. Lou, *Adv. Mater.* **2017**, *29*, 1703870; b) L. Zhuang, L. Ge, Y. Yang, M. Li, Y. Jia, X. Yao, Z. Zhu, *Adv. Mater.* **2017**, *29*, 1606793.
[12] a) I. Yamada, H. Fujii, A. Takamatsu, H. Ikeno, K. Wada, H. Tsukasaki, S. Kawaguchi, S. Mori, S. Yagi, *Adv. Mater.* **2017**, *29*, 1603004; b) G. Fu, X. Yan, Y. Chen, L. Xu, D. Sun, J.-M. Lee, Y. Tang, *Adv. Mater.* **2018**, *30*, 1704609.
[13] Y. Jin, H. Wang, J. Li, X. Yue, Y. Han, P. K. Shen, Y. Cui, *Adv. Mater.* **2016**, *28*, 3785.
[14] a) P. Chen, T. Zhou, M. Zhang, Y. Tong, C. Zhong, N. Zhang, L. Zhang, C. Wu, Y. Xie, *Adv. Mater.* **2017**, *29*, 1701584; b) Q. Xiong, Y. Wang, P.-F. Liu, L.-R. Zheng, G. Wang, H.-G. Yang, P.-K. Wong, H. Zhang, H. Zhao, *Adv. Mater.* **2018**, *30*, 1801450; c) Y. Liu, Q. Li, R. Si, G.-D. Li, W. Li, D.-P. Liu, D. Wang, L. Sun, Y. Zhang, X. Zou, *Adv. Mater.* **2017**, *29*, 1606200.
[15] J. Huang, Y. Sun, Y. Zhang, G. Zou, C. Yan, S. Cong, T. Lei, X. Dai, J. Guo, R. Lu, Y. Li, J. Xiong, *Adv. Mater.* **2018**, *30*, 1705045.
[16] M.-S. Balogun, W. Qiu, Y. Huang, H. Yang, R. Xu, W. Zhao, G.-R. Li, H. Ji, Y. Tong, *Adv. Mater.* **2017**, *29*, 1702095.
[17] H.-F. Wang, C. Tang, B. Wang, B.-Q. Li, Q. Zhang, *Adv. Mater.* **2017**, *29*, 1702327.
[18] a) H.-F. Wang, C. Tang, B.-Q. Li, Q. Zhang, *Inorg. Chem. Front.* **2018**, *5*, 521; b) Y. F. Zeng, L. Chen, R. Chen, Y. Wang, C. Xie, T. Li, L. Huang, S. Y. Wang, *J. Mater. Chem. A* **2018**, https://doi.org/10.1039/C8TA08149B.
[19] a) K. Xiang, J. Guo, J. Xu, T. Qu, Y. Zhang, S. Chen, P. Hao, M. Li, M. Xie, X. Guo, W. Ding, *ACS Appl. Energy Mater.* **2018**, *1*, 4040; b) L. Peng, J. Wang, Y. Nie, K. Xiong, Y. Wang, L. Zhang, K. Chen, W. Ding, L. Li, Z. Wei, *ACS Catal.* **2017**, *7*, 8184.
[20] C. Tang, L. Zhong, B. Zhang, H.-F. Wang, Q. Zhang, *Adv. Mater.* **2018**, *30*, 1705110.
[21] H. Xu, Z.-X. Shi, Y.-X. Tong, G.-R. Li, *Adv. Mater.* **2018**, *30*, 1705442.
[22] a) Z. Wen, S. Ci, F. Zhang, X. Feng, S. Cui, S. Mao, S. Luo, Z. He, J. Chen, *Adv. Mater.* **2012**, *24*, 1399; b) C. Hu, L. Zhang, Z.-J. Zhao, J. Luo, J. Shi, Z. Huang, J. Gong, *Adv. Mater.* **2017**, *29*, 1701820.
[23] a) X. Zou, Y. Liu, G.-D. Li, Y. Wu, D.-P. Liu, W. Li, H.-W. Li, D. Wang, Y. Zhang, X. Zou, *Adv. Mater.* **2017**, *29*, 1700404; b) X.-F. Lu, L.-F. Gu, J.-W. Wang, J.-X. Wu, P.-Q. Liao, G.-R. Li, *Adv. Mater.* **2017**, *29*, 1604437; c) S. Chen, J. Duan, M. Jaroniec, S.-Z. Qiao, *Adv. Mater.* **2014**, *26*, 2925; d) B. Liu, Y. Wang, H.-Q. Peng, R. Yang, Z. Jiang, X. Zhou, C.-S. Lee, H. Zhao, W. Zhang, *Adv. Mater.* **2018**, *30*, 1803144.
[24] K. Xu, H. Cheng, H. Lv, J. Wang, L. Liu, S. Liu, X. Wu, W. Chu, C. Wu, Y. Xie, *Adv. Mater.* **2018**, *30*, 1703322.
[25] J. Zhang, T. Wang, D. Pohl, B. Rellinghaus, R. Dong, S. Liu, X. Zhuang, X. Feng, *Angew. Chem., Int. Ed.* **2016**, *55*, 6702.
[26] L.-A. Stern, L. Feng, F. Song, X. Hu, *Energy Environ. Sci.* **2015**, *8*, 2347.
[27] B. Konkena, J. Masa, A. J. R. Botz, I. Sinev, W. Xia, J. R. Koßmann, R. Drautz, M. Muhler, W. Schuhmann, *ACS Catal.* **2017**, *7*, 229.
[28] X. Ji, S. Hao, F. Qu, J. Liu, G. Du, A. M. Asiri, L. Chen, X. Sun, *Nanoscale* **2017**, *9*, 7714.
[29] K. S. Novoselov, A. Mishchenko, A. Carvalho, A. H. Castro Neto, *Science* **2016**, *353*, aac9439.
[30] A. K. Geim, I. V. Grigorieva, *Nature* **2013**, *499*, 419.
[31] S. Jin, *ACS Energy Lett.* **2017**, *2*, 1937.
[32] C. Hu, L. Zhang, Z.-J. Zhao, A. Li, X. Chang, J. Gong, *Adv. Mater.* **2018**, *30*, 1705538.
[33] a) J. Chang, Q. Lv, G. Li, J. Ge, C. Liu, W. Xing, *Appl. Catal., B* **2017**, *204*, 486; b) R. Gao, G.-D. Li, J. Hu, Y. Wu, X. Lian, D. Wang, X. Zou, *Catal. Sci. Technol.* **2016**, *6*, 8268.
[34] a) Z. Liu, R. Ma, M. Osada, K. Takada, T. Sasaki, *J. Am. Chem. Soc.* **2005**, *127*, 13869; b) T. Wang, J. Wu, Y. Liu, X. Cui, P. Ding, J. Deng, C. Zha, E. Coy, Y. Li, *Energy Storage Mater.* **2019**, *16*, 24.
[35] a) Y. Zhu, G. Chen, Y. Zhong, Y. Chen, N. Ma, W. Zhou, Z. Shao, *Nat. Commun.* **2018**, *9*, 2326; b) Z. Cui, Y. Li, G. Fu, X. Li, J. B. Goodenough, *Adv. Mater.* **2017**, *29*, 1702385; c) C. Guo, Y. Zheng, J. Ran, F. Xie, M. Jaroniec, S.-Z. Qiao, *Angew. Chem., Int. Ed.* **2017**, *56*, 8539; d) X. Wang, L. Yu, B. Y. Guan, S. Song, X. W. Lou, *Adv. Mater.* **2018**, *30*, 1801211; e) C. Zhu, A.-L. Wang, W. Xiao, D. Chao, X. Zhang, N. H. Tiep, S. Chen, J. Kang, X. Wang, J. Ding, J. Wang, H. Zhang, H. J. Fan, *Adv. Mater.* **2018**, *30*, 1705516; f) S. Chen, Z. Kang, X. Hu, X. Zhang, H. Wang, J. Xie, X. Zheng, W. Yan, B. Pan, Y. Xie, *Adv. Mater.* **2017**, *29*, 1701687; g) T. Odedairo, X. Yan, X. Yao, K. Ostrikov, Z. Zhu, *Adv. Mater.* **2017**, *29*, 1703792; h) X. Zhu, T. Jin, C. Tian, C. Lu, X. Liu, M. Zeng, X. Zhuang, S. Yang, L. He, H. Liu, S. Dai, *Adv. Mater.* **2017**, *29*, 1704091; i) S. Yin, W. Tu, Y. Sheng, Y. Du, M. Kraft, A. Borgna, R. Xu, *Adv. Mater.* **2018**, *30*, 1705106; j) P. Cai, J. Huang, J. Chen, Z. Wen, *Angew. Chem., Int. Ed.* **2017**, *56*, 4858; k) L. Xu, Q. Jiang, Z. Xiao, X. Li, J. Huo, S. Wang, L. Dai, *Angew. Chem., Int. Ed.* **2016**, *55*, 5277.
[36] a) C. Tang, H.-F. Wang, H.-S. Wang, F. Wei, Q. Zhang, *J. Mater. Chem. A* **2016**, *4*, 3210; b) M. S. Burke, M. G. Kast, L. Trotochaud, A. M. Smith, S. W. Boettcher, *J. Am. Chem. Soc.* **2015**, *137*, 3638; c) D. Friebel, M. W. Louie, M. Bajdich, K. E. Sanwald, Y. Cai, A. M. Wise, M.-J. Cheng, D. Sokaras, T.-C. Weng, R. Alonso-Mori, *J. Am. Chem. Soc.* **2015**, *137*, 1305.
[37] O. Mabayoje, A. Shoola, B. R. Wygant, C. B. Mullins, *ACS Energy Lett.* **2016**, *1*, 195.
[38] T. Wang, G. Nam, Y. Jin, X. Wang, P. Ren, M. G. Kim, J. Liang, X. Wen, H. Jang, J. Han, Y. Huang, Q. Li, J. Cho, *Adv. Mater.* **2018**, *30*, 1800757.
[39] J. Duan, S. Chen, A. Vasileff, S. Z. Qiao, *ACS Nano* **2016**, *10*, 8738.
[40] B.-Q. Li, S.-Y. Zhang, C. Tang, X. Cui, Q. Zhang, *Small* **2017**, *13*, 1700610.
[41] J. Yang, G. Zhu, Y. Liu, J. Xia, Z. Ji, X. Shen, S. Wu, *Adv. Funct. Mater.* **2016**, *26*, 4712.
[42] A. Gupta, W. D. Chemelewski, C. Buddie Mullins, J. B. Goodenough, *Adv. Mater.* **2015**, *27*, 6063.
[43] a) W. Chen, H. Wang, Y. Li, Y. Liu, J. Sun, S. Lee, J.-S. Lee, Y. Cui, *ACS Cent. Sci.* **2015**, *1*, 244; b) A. M. Wiltrout, C. G. Read, E. M. Spencer, R. E. Schaak, *Inorg. Chem.* **2016**, *55*, 221.